www.czasopisma.pan.pl PAN POLSKA AKADEMIA NAUK www.journals.pan.pl

Arch. Metall. Mater. **70** (2025), 4, 1507-1513

DOI: https://doi.org/10.24425/amm.2025.156231

XIAOHUA LI[1], WENBING LI[1], RUI WANG[1], ENSHUN PING[2], SHAOFENG YANG[1*]

EFFECT OF DIFFERENT AlSi CONTENT ON MICROSTRUCTURE AND MAGNETIC PROPERTIES OF FeCoNi(AlSi)$_X$ HEA

This study aimed to design and prepare FeCoNi $(AlSi)_{0.2,0.4,0.6}$ high-entropy alloy (HEA) magnetic powder and bulk by MA and spark plasma sintering(SPS), and to investigate the effects of AlSi variations on the microstructure evolution and magnetic properties of HEAs. A decrease in AlSi content promoted the precipitation of stratification faults (SFs) and twins from the face-centered cubic matrix. The addition of AlSi nonmagnetic elements and the formation of SFs and twins had obvious effects on the magnetic properties of the HEA. FeCoNi$(AlSi)_{0.4}$ had excellent magnetic properties with 140.26±0.05 emu/g magnetic saturation (M_s) and 1.35±0.02 Oe coercivity field (H_c) and the excellent magnetic properties are due to the thinning effect of the single atomic layer twin boundary on the magnetic domain and the short-range magnetic domain bonding effect between the magnetic domains. The results of this study will expand the design and application of high-entropy alloys in the field of high-performance magnetic materials.

Keywords: HEA; Spark Plasma Sintering; Twins; Magnetic Properties

1. Introduction

High-entropy alloys (HEAs) based on ferromagnetic elements (Fe, Co, and Ni) have attractive magnetic properties besides the common superior properties, such as high strength, high hardness, wear resistance, corrosion resistance, and high-temperature stability [1-2]. The high-entropy magnetic alloy with relatively higher Curie temperatures, excellent saturation magnetic induction strength, and low coercivity is expected to replace brittle Fe-Co alloy, Fe-Si alloy with a high eddy-current loss, and bulk metallic glasses with structural instability. According to recent studies, The FeCoNi system HEAs with a single FCC crystal structure have high saturation magnetisation (M_s), high electrical resistivity and malleability, low coercivity (H_c), and such as FeCoNi$(CuAl)_x$, CoCuFeMnNi, FeCoNiAlCr_x and FeCoNi$(MgSi)_x$, etc. [3-5]. Lu et al. indicated that the as-cast Fe_2CoNi $AlSi)_x$ HEA exhibits a more superior comprehensive soft magnetic performance [6]. Zuo et al. showed that the Al or Si content has an influence on the M_s and electrical resistivity ρ for the FeNiCo alloy [7]. In addition, the advantages of Spark plasma sintering over conventional techniques for preparing magnetic HEAs are summarized as higher heating rate, lower sintering temperature, uniform composition [8-10].

Previous researchers focused on regulating the magnetic properties of HEAs by changing the types or proportions of alloying elements, but did not consider the relationship between alloying elements and the crystal structure of the alloys and the magnetic properties of the alloys. The addition of Group (3-4)A elements, such as Al and Si, can increase the stacking fault energy of the alloy, leading to the evolution of the crystal structure of the material. Therefore, the present study focused on the effect of AlSi content on the microstructure and magnetic properties of FeCoNi$(AlSi)_x$ (x = 0.2, 0.4, and 0.6, x is atomic ratios) HEA.

2. Experimental Procedure

High-purity (99.9%) Fe, Ni, Co, Al, and Si powders were used to produce FeCoNi$(AlSi)_x$ HEAs with unequal atomic ratios. Mechanical alloying had been vacuumed (residual cell pressure <10 Pa) and filled with high purity argon atmosphere for up to 40 and 5 h in C_2H_5OH (YXQM-4L-Planetary ball mill, 350 rpm, Stainless steel tanks with stainless steel balls, and a ball(400 g)-to-powder(50 g) weight ratio of 8:1). Then, a layer of silica was coated on the surface of HEA particles by liquid-phase in situ reduction [mixed solution: TEOS$(Si(OC_2H5)_4$,

[1] TIANJIN KEY LABORATORY OF HIGH PERFORMANCE PRECISION FORMING TECHNOLOGY AND EQUIPMENT, TIANJIN 300222, CHINA
[2] DOWNHOLE TECHNOLOGY SERVICE COMPANY, CNPC BOHAI DRILLING ENGINEERING COMPANY LIMITED, TIANJIN 300280, CHINA

* Corresponding author: yangshf@njit.edu.cn

C_2H_5OH, $NH_3{\cdot}H_2O$, and deionized water and specific amounts of C_2H_5OH/H_2O, $Si(OC_2H_5)_4$, and $NH_3{\cdot}H_2O$ were added to the ball mill tank and milled for 5 h. The prepared powders were consolidated using SPS in a 20-mm graphite die with an axial pressure of 30 MPa and at 1050°C for 5 min (residual cell pressure <5 Pa, room temperature to 500°C for 5min, 500°C to 800°C for 3 min and 800°C to 1050°C for 3 min, and then cooled in a graphite die).

The phase structures were investigated using x-ray diffraction (XRD, Bruker D8 ADVANCE). Thin-foil specimens prepared by twin-jet electropolishing and the dispersed powder adhered to the copper mesh had been observed under a 200 keV transmission electron microscope (TEM, JOEL JEM-2100). The magnetic behavior and magnetic domains inside the material of $FeCoNi(AlSi)_x$ were tested by a vibrant sample magnetometer test (WSM, LakeShore-7400s) and lorentz transmission electron microscopy (LTEM, JEM-2100F).

3. Results and discussion

The XRD patterns of powders and the bulk SPS-ed SiO_2-$FeCoNi(AlSi)_x$ HEAs are illustrated in Fig. 1. The results showed that the $FeCoNi(AlSi)_x$ HEA powder were composed of a single FCC phase (PDF:47-1406, Fm-3m [225], $Cu_{0.81}Ni_{0.19}$) and amorphous silica with no obvious diffraction peak (Fig. 1a); however, after the sintering of SiO_2-$FeCoNi(AlSi)_x$ HEAs (Fig. 1b), obvious silica crystals were observed but with no phase evolution of the single FCC alloy phase. Similarly, the TEM analysis of the alloy powder revealed that the electron diffraction analysis also showed that the SiO_2 generated in situ had a relatively low crystallinity. Fig. 2(a) is the TEM patterns of the as-milled SiO_2-$FeCoNi(AlSi)_x$ HEA powders and the diffuse halo ring in Fig. 2(b) is a characteristic feature of amorphous materials, distinct from the sharp diffraction spots/rings of crystalline phases. As shown in Fig. 2(c), the thickness of the SiO_2 shell on the HEA surface was about 3-5 nm. Furthermore, TEM/EDX analysis confirmed that the main surface composition of SiO_2-$FeCoNi(AlSi)_{0.2}$ HEA particles is SiO_2, because the ratio of oxygen to silicon atoms is approximately 2:1(O, 63.08 at.% and Si,31.69 at.%, Fig. 3).

The formation theory of high-entropy alloys indicates that the thermodynamic parameters of HEAs include mixing entropy (ΔS), mixing enthalpy (ΔH), atomic size difference calculation parameter (Ω), and valence electron concentration (VEC). The relevant feature parameters of the $FeCoNi(AlSi)_x$ alloy system were calculated using the following equations [11]:

$$\Delta S_{mix} = -R \cdot \sum_{i=1}^{n} c_i \ln c_i \tag{1}$$

$$\Delta H_{mix} = \sum_{i=1, i\neq j}^{n} \Omega_{ij} c_i c_j \tag{2}$$

$$\delta = \sqrt{\sum_{i=1}^{n} c_i \left(1 - \frac{r_i}{\left(\sum_{i=1}^{n} c_i r_i\right)}\right)^2} \tag{3}$$

$$\Omega = \frac{T_m \Delta S_{mix}}{|\Delta H_{mix}|} \tag{4}$$

$$VEC = \sum_{i=1}^{n} C_i \left(VEC\right)_i \tag{5}$$

where $\Omega_{ij} = 4\Delta H_{ij}^{mix}$ is the mixing enthalpy for the binary equiatomic *ij* alloys, while n, c_i, c_j and r_i are the number of elements, mole fractions of the i^{th} and j^{th} components' elements, and the average atomic radius, and where R is the ideal gas constant, T_m is the average melting point of the HEA alloy, and $(VEC)_i$ is the VEC of component i, respectively.

TABLE 1 presents the ΔH_{ij}^{mix} values for the binary ij alloys incorporated in the $FeCoNi(AlSi)_x$ alloy. The formation of FCC crystals in multi-principal component alloys was mainly due to a high entropy effect. The calculated values of ΔS, ΔH, δ, Ω, and VEC (Calculation formulas ref. [5,6]) for $FeCoNi(AlSi)_x$ were determined as in TABLE 2. These results aligned with the findings of Zhang and Guo et al. [5,6], indicating the formation of $FeCoNi(AlSi)_x$ single FCC phase. In addition, TEOS($Si(OC_2H_5)_4$

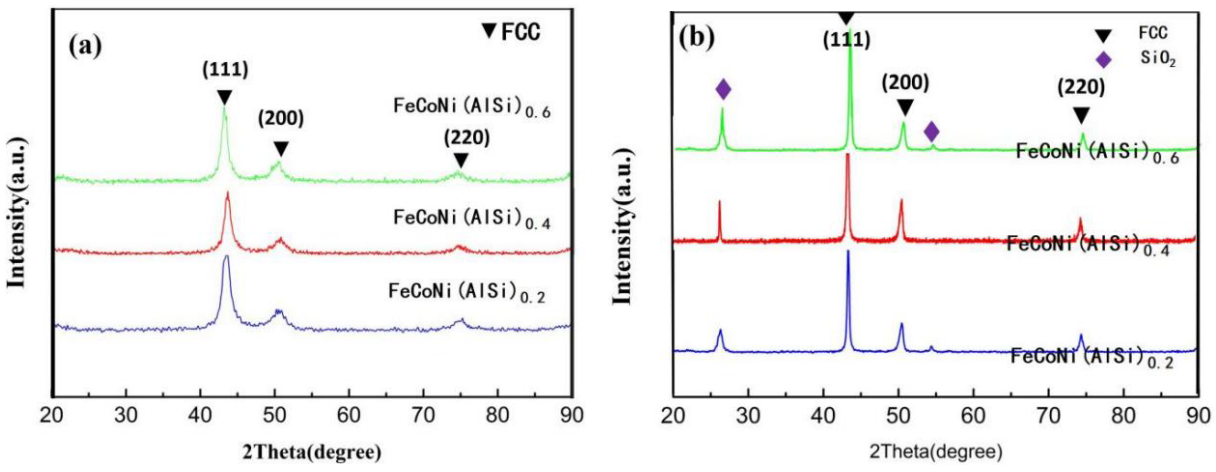

Fig. 1. XRD patterns of powders (a) and the bulk SPS-ed (b) of SiO_2-$FeCoNi(AlSi)_x$ HEAs

decomposed into the siloxy group ($(Si\text{-}O\text{-}Si)_{n\text{-}x}$-$(Si\text{-}OH)_x$) and the roasted Si hydroxyl $(Si\text{-}OH)_x$ was converted into crystalline SiO_2 in the environment of C_2H_5OH and $NH_3{\cdot}H_2O$.

TABLE 1

$(VEC)_i$ and ΔH_{ij}^{mix} (KJ/mol) for the binary ij alloys incorporated in the $FeCoNi(AlSi)_x$ alloy [12]

Elements	Fe	Co	Ni	Si	Al	$(VEC)_i$
Fe	–	–1	–2	–35	–11	8
Co	–1	–	0	–38	–19	9
Ni	–2	0	–	–40	–22	10
Si	–35	–38	–40	–	–19	4
Al	–11	–19	–22	–19	–	3

Figs. 4, 5 and 6 showed the magnetic properties of SiO_2-$FeCoNi(AlSi)_x$ and $FeCoNi(AlSi)_x$ HEAs which are listed in TABLE 3. Both the $FeCoNi(AlSi)_x$ powders (Figs. 4a, 5a, and 6a) and the bulk of SiO_2-$FeCoNi(AlSi)_{0.2}$ (Fig. 4f) and SiO_2-$FeCoNi(AlSi)_{0.6}$ (Fig. 6f) HEAs showed semi hard magnetism. Interestingly, the SiO_2-$FeCoNi\ (AlSi)_{0.4}$ showed a magnetic with M_s of 140.26±0.05 emu/g and H_c of 1.35±0.02 Oe (Figs. 5d and 5f).

Previous studies have shown that the microstructure in crystals, including layering faults and defects, can significantly affect the coercive force of materials [9,10]. The stacking fault energy of the system increases with an increase in the AlSi content with a larger relative atomic radius, lead-

TABLE 2

The values of ΔS_{mix}, ΔH_{ij}^{mix}, δ, Ω, and VEC of HEAs

Alloy compounds	ΔS_{mix}	ΔH_{ij}^{mix}	δ	Ω	VEC
$FeCoNi(AlSi)_{0.2}$	10.87 J/mol	–8.97 KJ/mol	3.46%	1.87	8.87
$FeCoNi(AlSi)_{0.4}$	11.75 J/mol	–9.01 KJ/mol	3.88%	1.49	8.76
$FeCoNi(AlSi)_{0.6}$	12.31 J/mol	–9.36 KJ/mol	4.07%	1.37	8.67

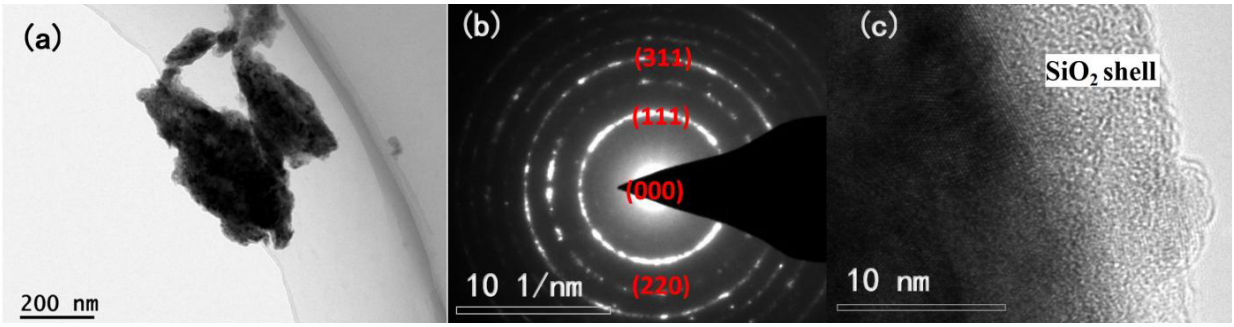

Fig. 2. TEM patterns of SiO_2-$FeCoNi(AlSi)_{0.2,0.4,0.6}$ HEA powders:(a) is particle morphology, (b)is the SAED pattern and (c) is the surface of the shell

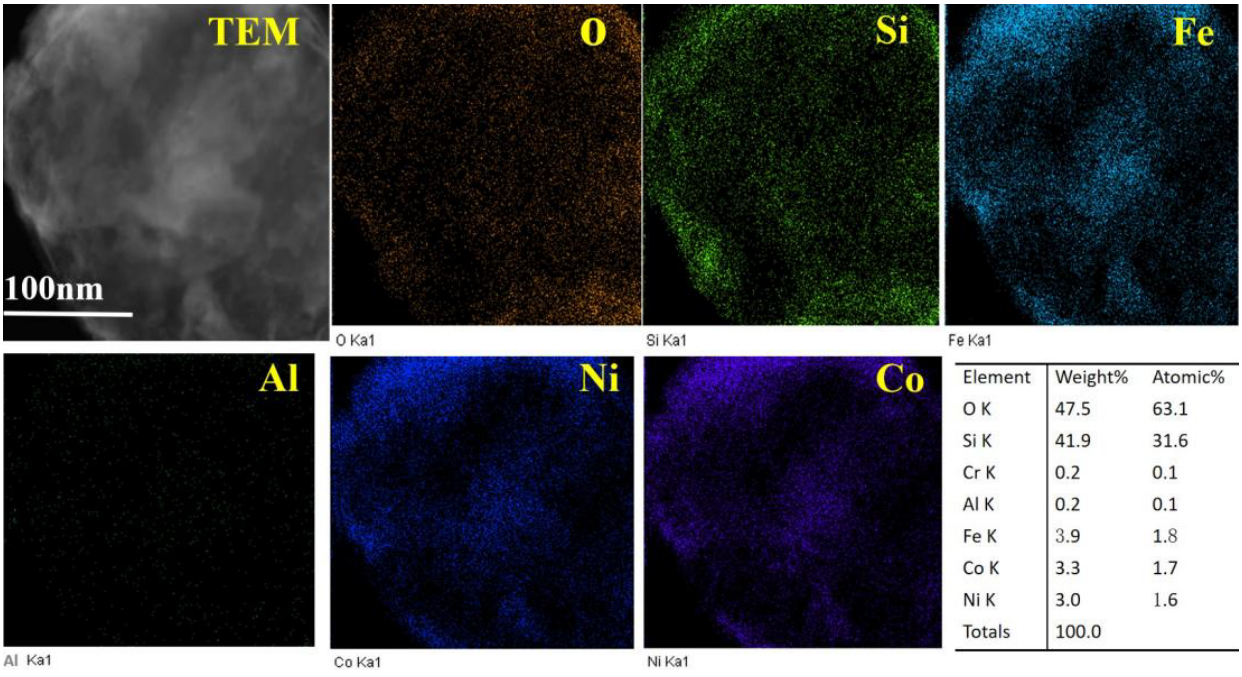

Fig. 3. TEM-EDX mapping of SiO_2-$FeCoNi(AlSi)_{0.2}$ HEA particles

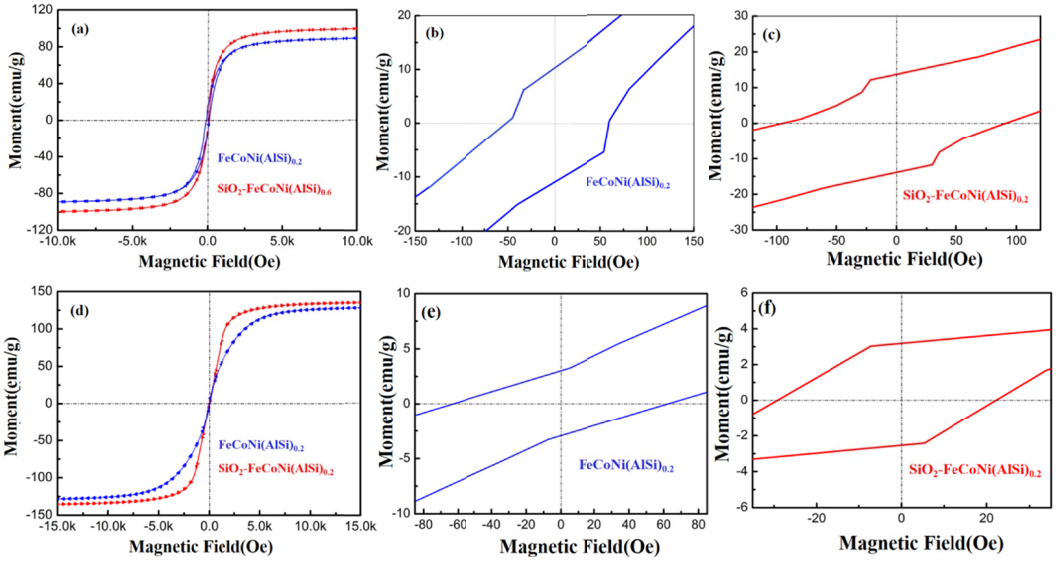

Fig. 4. Magnetic properties of the powders (a, b, c) and the bulks (d, f, e) of SiO_2- $FeCoNi(AlSi)_{0.2}$

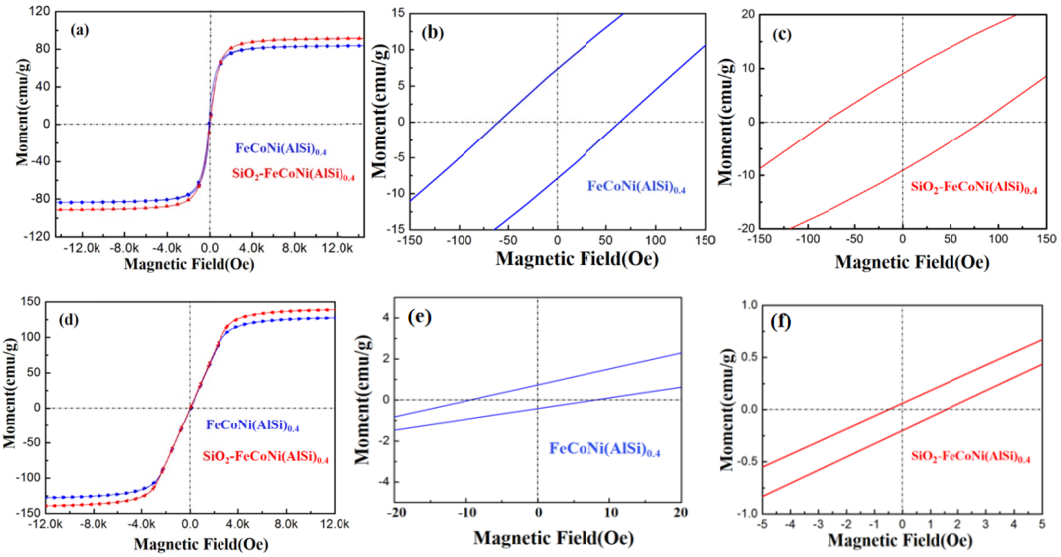

Fig. 5. Magnetic properties of the powders (a, b, and c) and the bulks (d, f, and e) of SiO_2- $FeCoNi(AlSi)_{0.4}$

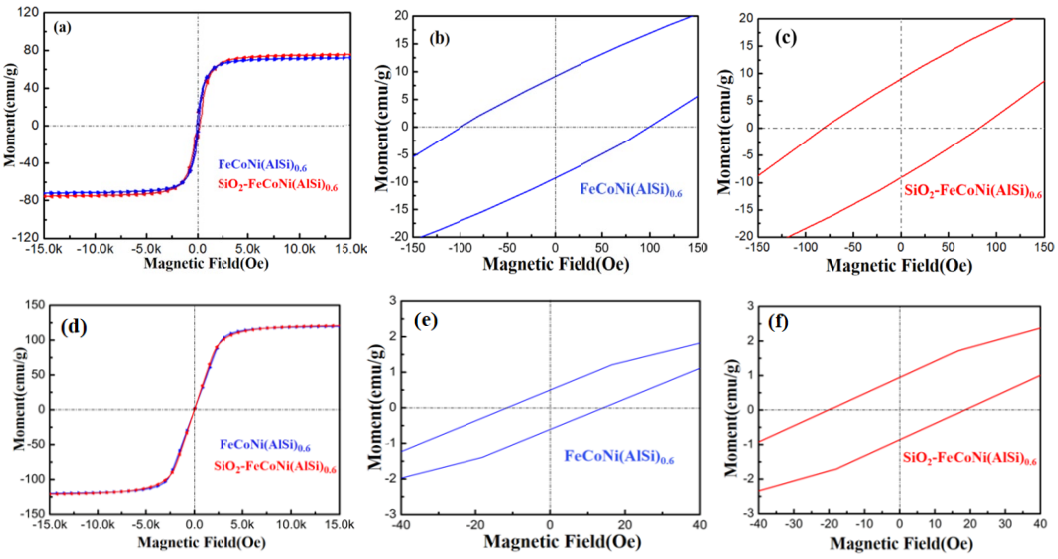

Fig. 6. Magnetic properties of the powders (a, b, and c) and the bulks (d, f, and e) of SiO_2- $FeCoNi(AlSi)_{0.6}$

TABLE 3

Magnetic of $FeCoNi(AlSi)_x$ HEAs compare with ref.

Composition (at.%)	M_s (emu/g)	H_c (Oe)	Ref.
$FeCoNi(AlSi)_{0.2}$ Particle	87.63±0.05	52.72±0.02	This work
SiO_2-$FeCoNi(AlSi)_{0.2}$ Particle	98.35±0.05	87.41±0.02	This work
Bulk $FeCoNi(AlSi)_{0.2}$	127.81±0.05	62.33±0.02	This work
Bulk SiO_2-$FeCoNi(AlSi)_{0.2}$	133.72±0.05	28.25±0.02	This work
$FeCoNi(AlSi)_{0.4}$ Particle	82.73±0.05	63.47±0.02	This work
SiO_2-$FeCoNi(AlSi)_{0.4}$ Particle	90.64±0.05	76.33±0.02	This work
Bulk $FeCoNi(AlSi)_{0.4}$	127.87±0.05	8.24±0.02	This work
Bulk SiO_2-$FeCoNi(AlSi)_{0.4}$	140.26±0.05	1.35±0.02	This work
$FeCoNi(AlSi)_{0.6}$ Particle	74.66±0.05	105.84±0.02	This work
SiO_2-$FeCoNi(AlSi)_{0.6}$ Particle	77.37±0.05	77.62±0.02	This work
Bulk $FeCoNi(AlSi)_{0.6}$	123.58±0.05	12.37±0.02	This work
Bulk SiO_2-$FeCoNi(AlSi)_{0.6}$	124.26±0.05	17.83±0.02	This work
$(FeCoNi)_{70}Ti_{10}B_{20}$ Particle	119.2	13.4	13
CoNiMnGa Arc melting	115.92	25	14
Bulk CuCrFeTiNi	64.38	4.63	6,15

ing to a decrease in the deformation fault generation and twin formation ability. The stacking fault deformation zone of 10-15 layers appears in SiO_2-$FeCoNi(AlSi)_{0.2}$ (Fig. 7(a)), whereas the deformation twin boundary of 1-3 layers exists in SiO_2-$FeCoNi(AlSi)_{0.4}$ showed in Fig. 7(b). Forming twins and stacking faults in SiO_2-$FeCoNi(AlSi)_{0.6}$, which has the largest stacking fault energy(Fig. 7(c)), is challenging. Therefore, SiO_2-$FeCoNi(AlSi)_{0.2}$ has higher M_s and H_c due to the highest content of ferromagnetic elements, and the wide stacking misalignment deformation area leads to the effect of layer misalignment on domain wall pinning.

Compared with the structure of the two others contains fewer ferromagnetic elements and higher stacking fault energy, making it challenging to produce deformation twins, leading to lower M_s and increased H_c caused by large magnetic domains. However, for SiO_2- $FeCoNi(AlSi)_{0.4}$ with reasonable content of ferromagnetic elements, the deformation faults and twins formed deformation regions with only one to three layers. This could not limit the movement of magnetic domains except for the segmentation and refinement of magnetic domains. Compared with the magnetic high-entropy alloys currently studied, such as FeNiMnCuCo (M_s, 79.64 emu/g and H_c, 32.44 Oe), $FeCoNiCr_{0.2}Si_{0.2}$ (M_s, 98.11 emu/g and H_c, 2.36 Oe), $FeCoNiSi_{0.75}$ (M_s, 80.5±0.05 emu/g and H_c, 56.95Oe) and $Co_4Fe_2Al_{1.5}Mn_{1.5}$ (M_s, 161.3emu/g and H_c,1.9Oe)[13-16], SiO_2-$FeCoNi(AlSi)_{0.4}$ had better M_s and lower H_c.

In order to further study the distribution and evolution of magnetic domain walls in the single atom twin boundary of HEAs, the local domain structures of the twin was observed by LTEM under different magnetic fields(Fresne-overfocus mode, 200 Oe and 400 Oe) as shown in Fig. 8. The selected twin structure region is shown in Fig. 8(a). The separation of magnetic domai n structure by twin boundary in demagnetization state is shown in Fig. 8(b), and the domain walls of twin-to-grain cutting are almost parallel to the twin grain boundary, and the white contrast domain walls at the grain boundary are mostly distributed along the grain boundary. The magnetized sample rod was used to field the twin SiO_2-$FeCoNi(AlSi)_{0.4}$ transmitted sample in situ, and the direction of the external magnetic field was parallel to the sample surface, as shown by the yellow arrows in (c) and (d) in Fig. 8. As shown in Fig. 8(c), when a field of 200 Oe was applied to the sample, the twin domain walls shifted significantly and widened. When the external magnetic field was further increased to 400 Oe, the strip magnetic domain walls formed by twins moved more easily and continued to widen. The reason for the formation of transgranular domains is that the magnetic

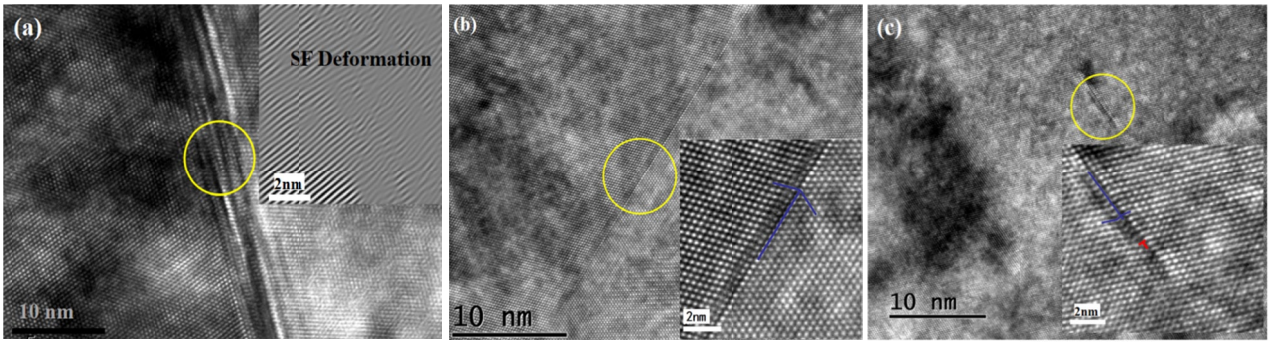

Fig. 7. HRTEM micrographs revealing deformation twinning , (a)is SiO_2-$FeCoNi(AlSi)_{0.2}$, (b) is SiO_2-$FeCoNi(AlSi)_{0.4}$ and (c) is SiO_2-$FeCoNi(AlSi)_{0.6}$

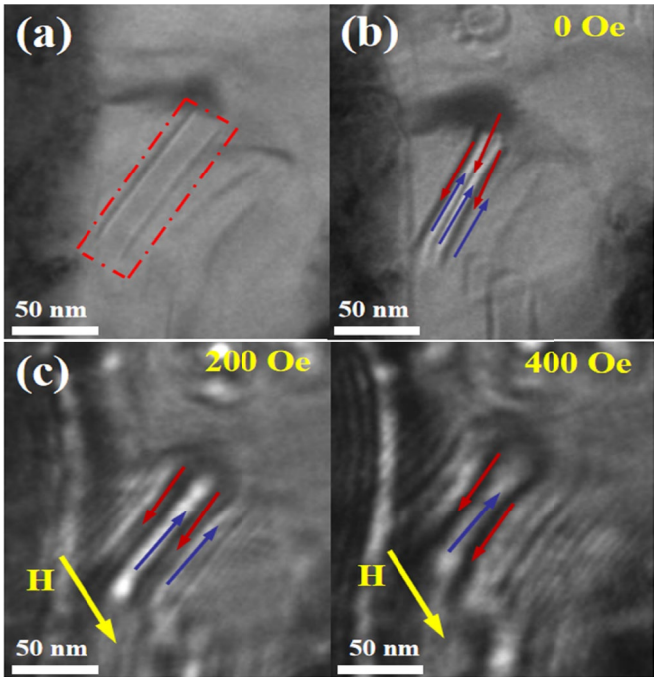

Fig. 8. Local domain structures of nanotwin in SiO_2-FeCoNi$(AlSi)_{0.4}$ HEAs, (a) in focus and (b) over focus LTEM images of the demagnetized samples, (c) and (d) over focus images of magnetized states under different external fields

domain splits due to the change of crystal orientation centered on the twin axis, which plays a role in thinning the magnetic domain. However, the twin grain boundary thickness is only a single atomic plane (Fig. 7b), such a crystal defect cannot cause a pinning effect on the fine twin magnetic domain, so there is a short-range exchange coupling between the mother phase and the twin crystal. Therefore, the parent phase and the twin phase grains of the multi-twin magnet are almost coupled together, so the appearance of the transgranular domains of the multi-twin magnet is mainly due to the exchange coupling between the grains. Twin crystals are conducive to thinning magnetic domains, forming nanolamellae magnetic domains, which have positive effects on improving the saturation magnetic induction intensity of SiO_2-FeCoNi$(AlSi)_{0.4}$ of magnets, while short-range exchange coupling makes the domain walls move easily under the external magnetic field, which is beneficial to the coercivity of magnets. Comparing the microstructure of SiO_2-FeCoNi$(AlSi)_{0.2}$ and SiO_2-FeCoNi$(AlSi)_{0.6}$ (Figs. 7a and 7c), SiO_2-FeCoNi$(AlSi)_{0.2}$ did not form a complete twin structure, and the magnetic domain could not be refined by the half-twin boundary. The relative SiO_2-FeCoNi$(AlSi)_{0.6}$ formed a layered fault structure with multiple atomic layers, which disrupted the magnetic domains and also effectively fixed the domain wall movement, thus increasing the coercivity.

4. Conclusions

(1) The SiO_2-FeCoNi$(AlSi)_x$ HEAs with x = 0.2, 0.4, and 0.6 was prepared by MA and SPS. TEM/EDX analysis confirms that high entropy alloy particles with core-shell structure can be obtained by liquid phase reduction technique.

(2) The new composition of the class of SiO_2-FeCoNi$(AlSi)_x$ bulk HEAs with x = 0.4 led to much better soft magnetic performance compared with the other two alloys.

(3) The obtained higher M_s and lower coercivity were mainly related to the deformation regions with narrow stacking fault and twin boundary, which caused the thinning of magnetic domains but did not affect the movement of fine magnetic domains.

(4) The single atomic layer twin boundary in SiO_2-FeCoNi $(AlSi)_{0.4}$ has no napping effect on the magnetic domain wall, which is conducive to the formation of short-range magnetic coupling effect between magnetic domains, while the multi-atomic layer fault crystal in SiO_2-FeCoNi$(AlSi)_{0.6}$ defects exert the napping effect, which increases the coercivity.

Acknowledgements

The authors gratefully acknowledge the Opening Project of Guangdong Provincial Key Laboratory for Processing and Forming of Advanced Metallic Materials, South China University of Technology (GJ 202406) and the Research Program Project of Tianjin Education Commission (Grant No.2023ZD037).

REFERENCES

[1] P. Kumari, P. Gupta, R.K. Mishra, M.S. Ahmad, A comprehensive review: recent progress on magnetic high entropy alloys and oxides. J. Magn. Magn. Mater. **554**, 169142 (2022). DOI: https://doi.org/10.1016/j.jmmm.2022.169142

[2] T.X. Kang, S.Y. Wu, M.L. Wang, Y.P. Lu, Novel $Fe_2CoNi(AlSi)_x$ high-entropy alloys with attractive soft magnetic and mechanical properties. Appl. Phys. A **127**, 829 (2021). DOI: https://doi.org/10.1007/s00339-021-04988-7

[3] K. Bora, S. Tuncay, A. Baris, Atomic configurations in mechanically alloyed amorphous $(FeCoNi)_{70}Ti_{10}B_{20}$ powders. J. All. Compd. **960**, 170667 (2023). DOI: https://doi.org/10.1016/j.jal lcom.2023.170667

[4] M. Zeraati, M.H.K. Feizabad, G.R. Khayati, An investigation of the magnetic, mechanical, and kinetic characteristics of Cu-CrFeTiNi high entropy alloy by mechanical alloying and spark plasma sintering. J. All. Compd. **958**, 170347 (2023). DOI: https://doi.org/10.1016/j.jallcom. 2023.170347

[5] V. Chaudhary, R. Chaudhary, R. Banerjee, Accelerated and conventional development of magnetic high entropy alloys. Mater. Today. **49**, 231-252 (2021). DOI: https://doi.org/10.1016/j.ma ttod.2021.03.018

[6] Y. Zhang, T.T. Zuo, Z. Tang, M.C. Gao, et al., Microstructures and properties of high-entropy alloys. Prog. Mater. Sci. **61**, 1-93 (2014). DOI: http://dx.doi.org/10.1016/j.pmat sci.2013.10.001

[7] T.T. Zuo, M. Zhang, P.K. Liaw, Y. Zhang, Processing effects on the magnetic and mechanical properties of $FeCoNiAl_{0.2}Si_{0.2}$ high

entropy alloys. Inter. J. Miner. Metall. Mater. **20**, 549-551 (2013). DOI: https://doi.org/10.1007/s12613-013-0764-x

[8] P. Sahu, S. Samal, V. Kumar, Microstructural, magnetic, and geometrical thermodynamic investigation of $FeCoNi(MnSi)_x$ (0.0, 0.1, 0.25, 0.5, 0.75, 1.0) high entropy alloys. Materialia **18**, 101133 (2021). DOI: https://doi.org/10.1016/j.mtla.2021.101133

[9] K.X. Zhou, B.R. Sun, G.Y. Liu, X.W. Li, S.W. Xin, P.K. Liaw, T.D. Shen, FeCoNiAlSi high entropy alloys with exceptional fundamental and application-oriented magnetism. Intermetallics. **122**, 106801 (2020). DOI: https://doi.org/10.1016/j.intermet.2020.106801

[10] M. Javdan, K. Gheisari, M. Reihanian, Mechanically alloyed $(FeCoNi)_{75}Cu_{25}$-xSix high entropy alloys: phase evaluation and magnetic properties. J. All. Compd. **952**, 170030 (2023). DOI: https://doi.org/10.1016/j.jallcom.2023.170030

[11] W. Gao, Y.Q. Dong, X.J. Jia, L.P. Yang, et al., Novel CoFeAlMn high-entropy alloys with excellent soft magnetic properties and high thermal stability. J. Mater. Sci. Tech. **153**, 22-31 (2023). DOI: https://doi.org/10.1016/j.jmst.2023.01.010

[12] N. Jahani, M. Reihanian, K. Gheisar, Alloying, Phases and magnetic behaviour of mechanically alloyed FeNiMnCu-based high entropy alloys. Mater. Sci. Tech. **39**, 1745-1759 (2023). DOI: https://doi.org/10.1080/02670836.2023.2180902

[13] L. Han, F. Maccari, I.R.S. Filho, et al., A mechanically strong and ductile soft magnet with extremely low coercivity. Nature. **608**, 310-316 (2022). DOI: https://doi.org/10.1038/s4158 6-022-04935-3

[14] H.Y. Chen, J.M. Gou, W.T. Jia, X. Song, T.Y. Ma, Origin of hard magnetism in Fe-Co-Ni-Al-Ti-Cu high-entropy alloy: chemical shape anisotropy. Acta Mater. **246**, 118702 (2023). DOI: https://doi.org/10.1016/j.actamat.2023.118702.

[15] A. Talaat, M.V. Suraj, K. Byerly, A. Wang, et al., Review on soft magnetic metal and inorganic oxide nanocomposites for power applications. J. All. Compd. **870**, 159500 (2021). DOI: https://doi.org/10.1016/j.jallcom.2021.159500

[16] R.F. Zhao, B. Ren, G.P. Zhang, Z.X. Liu, J.J. Zhang, Effect of Co ccontent on the phase transition and magnetic properties of $Co_xCrCuFeMnNi$ high-entropy alloy powders. J. Magn. Magn. Mater. **468**, 14-24 (2018). DOI: https://doi.org/10 .1016/j. jmmm.2018.07.072